Proceedings of 25th Annual Fellowship Symposium
Utah NASA Space Grant Consortium
May 6, 2019, Provo, UT, USA

CAVITATION INCEPTION AND PERFORMANCE OF A CENTRIFUGAL IMPELLER DURING START-UP

D. Tate Fanning *
Dept. of Mechanical Engineering
Brigham Young University
Provo, UT 84062
Email: tatefanning@byu.edu

ABSTRACT

Rapid acceleration of rocket engine turbopumps during start-up imparts significant transient effects to the resulting flow field, causing pump performance to vary widely when compared to quasi-steady operation. To improve turbopump design in response to the transient effects of start-up this paper presents a method to simulate turbopump start-up using CFD. Cavitating pump performance is initially evaluated using a simulation with a constant outlet pressure boundary condition. Based on the difference between simulation inlet pressure and target inlet pressure, the defined pressure on the outlet boundary condition is modified. This process is repeated until simulation inlet pressure is essentially constant during start-up. Using this simulation method, the performance of a centrifugal turbopump during start-up is simulated. Reasonable solution convergence is reached in one single phase and four cavitating simulation iterations. After these five simulation iterations, the average error between inlet pressure and inlet target pressure is 10%. *Cavitating simulation iterations* 3 *and* 4 *agree within* 11% *on average for inlet total pressure during startup,* 0.1% *on average for head coefficient,* 13% *on average for cavitation volume,* 20% *on average for flow coefficient, and* 2% *on average for RMS force on the impeller. The agreement between simulation iterations* 3 *and* 4 *suggests that a reasonable solution has been reached.*

*Address all correspondence to this author.

NOMENCLATURE

A_{LE} Impeller Leading Edge Area
D_{tip} Impeller Tip Diameter
F_{RMS} RMS Force
g Acceleration due to Gravity
$\dot{m}_{in}$ Inlet Mass Flow
P Total Pressure
P_{in} Inlet Total Pressure
$P_{in,\,target}$ Target Inlet Total Pressure
P_{out} Outlet Static Pressure
$P_{out,\,total}$ Outlet Total Pressure
P_{vapor} Vapor Pressure
Q Volume Flow Rate
t Time
U_{tip} Impeller Blade Tip Speed
V Volume
V_{vapor} Total Vapor Volume
ρ Density
ϕ Flow Coefficient, $\dot{m}_{inlet}/(\rho A_{LE} U_{tip})$
ψ Head Coefficient, $(P_{out,\,total} - P_{in})/(\rho U_{tip}^2)$
ω Rotational Rate

1 INTRODUCTION

Cavitation inception and the resulting effects on pump performance are typically considered during quasi-steady operation. This method of analysis can capture cavitation formation and instabilities and as well as performance of the pump for a constant rotational rate, which is typical

operation for most turbopumps. However, several applications require controlled operation from start-up to shutdown [1]. These unsteady operational parameters are characterized by rapidly increasing rotation rate, which generates substantial pressure fluctuations that cause additional transient effects in the formation and growth of cavitation that are not evident during quasi-steady operation. These additional transient effects during start-up are not insignificant and are governed mainly by the increasing rotational speed $d\omega/dt$ and the flow rate increase dQ/dt [2].

Various aspects of transient flow in centrifugal pumps have been explored for quite some time. Lefebvre measured the performance of a centrifugal pump during quasi-steady operation in addition to testing four different start-up profiles [1]. He found transient head to be considerably higher than the quasi-steady operation at the start of the transient operation due to impulsive pressure rise. However, head dropped and remain below the quasi-steady value for the rest of the start-up as the effects of the impulsive pressure decay. Tsukamoto found similar results in his experimental and theoretical study, and concluded that the period of head depression below quasi-steady values is due to the lag of circulation growth around the impeller vanes [3].

Additional efforts have further explored the transient start-up of an impeller experimentally [4–7]. Some have found that non-dimensional head is very high at the beginning of start-up, but falls rapidly and recovers to a final, stable value [8]. Others have investigated the response of of an impeller to sinusoidal variations in rotational speed and found the transient characteristics of the flow to deviate remarkably from the quasi-steady values [9]. Pressure and flowrate oscillations during transient start-up have been found to be generated by oscillating cavitation [10]. Transient behavior has been found to be caused by oscillating cavitation or water hammer with water column separation [11], with low frequency, high amplitude pressure oscillations occurring at high flow rates and a pressure decrease at the end of start-up occurring at lower flow rates [12]. Further work has been done that found the backflow region to exhibit a much lower extension during start-up than during steady state operation [13]. In addition to the body of experimental work, models to predict pump performance during cavitating fast start-ups [2, 14–16] have been developed.

These previous studies have focused on experimental work and theoretical models to describe centrifugal impeller performance during fast start up. Experimental data is exact, but studies are expensive and it is difficult to change impeller geometry quickly and easily. Theoretical models are useful, but do not necessarily predict the intricacies of a flow field generated by a novel impeller geometry. The purpose of this work is to simulate cavitating performance of a centrifugal impeller during fast start up using computational fluid dynamics (CFD). Simulating cavitating performance of a centrifugal impeller during start-up using CFD is a novel effort that offers results specific to the pump design that describe the complete flow field while providing potentially more accurate results than a general theoretical model and being less expensive than a complete experimental study.

2 CFD MODELING

A centrifugal impeller is the subject of numerical simulations here. The simulations were performed using the commercial software Star-CCM+ v11.04.010 which is capable of accurately modeling cavitation in pump systems.

2.1 Spatial Discretization

The geometry used in simulations here consists of a full annulus inlet pipe, centrifugal impeller and radial outlet. No volute design is considered here, as the main concern of this work is the simulation method rather than actual pump performance. However, this work does investigate the effect of cavitation formation just upstream of the impeller during fast start up. The pump computational domain is defined by a mesh generated in Star-CCM+. The mesh is comprised of 16.6×10^6 polyhedral cells, and a cross section of the full mesh is provided in Fig. 1. To better capture flow physics around the blade tips, refinement increases along the inlet pipe and near the impeller blades and hub, as seen in Fig. 2. The average y^+ value for the mesh is 73.

To test grid independence, a Richardson based error estimation using a safety factor of 1.25 [17, 18] was performed using quasi steady simulation results to determine the grid convergence index (GCI) using additional meshes of 8.94×10^6 and 25.5×10^6 cells. The resulting GCIs are included in Table 1 and provide an error band estimation for quasi steady pump operation. GCI_{12} shows the estimated error of the base mesh when compared to the more

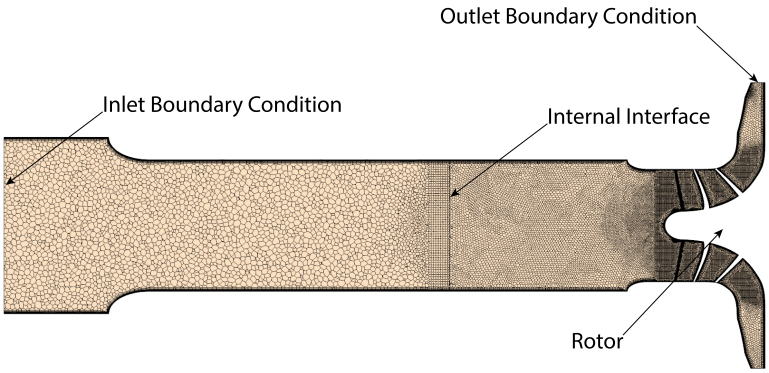

FIGURE 1: Mid-plane section of the mesh

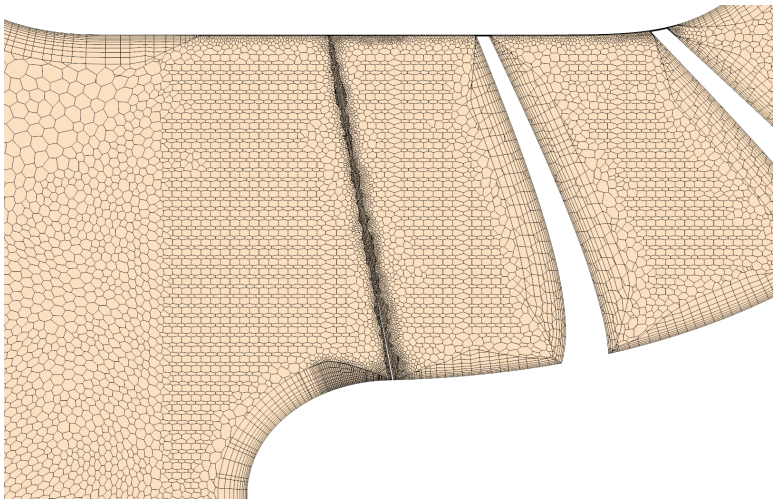

FIGURE 2: Tip detail of a mid-plane section of the mesh

refined mesh. GCI_{23} shows the estimated error of the base mesh when compared to the less refined mesh. Both error estimations using GCI are reasonably small, and indicate the baseline mesh is sufficiently refined and more refined meshes are not required to obtain reasonable simulation accuracy. Thus, for this work, all reported values are estimations with an error band of 2.3%.

2.2 Cavitation Model

A simple constant density equation of state model is used as the frame to describe single phase flow. Simulating pump performance in the single phase regime is done to provide pressure and velocity fields as initial conditions for cavitating simulations. An Eulerian multiphase volume of fluid method [19] is used to describe cavitation formation and flow with liquid water as the primary phase, and water vapor as the secondary phase. This cavitation modeling method uses a simplification of the general Rayleigh-Plesset equation and solves the single phase governing equation set for an equivalent fluid with physical properties defined as functions of constituent phases and volume fractions. Individual cavitation bubbles are not modeled with this approach. A Rayleigh-Plesset formulation that includes the influence of bubble growth acceleration along with viscous and surface tension effects is employed to model rate of vapor production.

In the volume of fluid model, a single set of momentum and turbulence equations are solved to find the distribution of the continuous phase. The dispersed phase is then modeled with a transport equation for the volume fraction [19]. The density and dynamic viscosity are calculated as functions of the physical properties of the constituent phase and its volume fraction.

TABLE 1: Grid convergence index comparison for three mesh sizes. These values loosely represent error bands for data extracted from the numerical simulations.

	%
GCI_{12}	0.62
GCI_{23}	2.31

2.3 Turbulence Model

The realizable k-ε model is used here to model turbulence. This model applies offers mesh flexibility by applying wall functions to model the boundary layer in the viscous sublayer if the wall $y^+ > 30$, and assumes the mesh density properly resolves the viscous sublayer for regions where the wall $y^+ < 30$. Despite the relatively large overall mesh size, the average y^+ of the mesh used here is not necessarily ideal, and wall functions are applied by the turbulence model to help offset the relative coarseness of the mesh to properly resolve the boundary layer.

Lundgreen modeled the flow physics of a similar computational setup of an axial inducer with a 7° tip blade angle during quasi-steady operation using the same turbulence and cavitation models with good agreement when compared to experimental data, predicting the cavitation number where head breakdown occurs within 1% of the experimentally observed value [20].

2.4 Boundary and Initial Condition Specification

The computational domain consists of two regions, joined by an internal interface boundary which is visible in Fig. 1. This boundary is located $2.8 * D_{tip}$ upstream of the leading edge of the impeller and separates the inlet pipe region with no rotating components and the rotor region, which contains surfaces that change rotational rate based on time.

Quasi-steady pump performance is often estimated with CFD simulations characterized by a constant rotation rate. A constant rotation rate is modeled in Star-CCM+ with a rotating reference frame or rigid body motion [21]. Rigid body motion moves the mesh cell vertices a fixed displacement per time step, and must be employed in a transient analysis. While this method is the most accurate approach to simulate impeller rotation, it can be very computationally expensive for a large mesh [21], like the one generated for this work. While less accurate, a rotating reference frame is less computationally intensive and provides a compromise between simulation accuracy and computational cost. For this reason, this work employs a rotating reference frame to simulate rotation. The rotor surfaces, which are defined as no slip walls, are the only parts defined to be in the rotating reference frame, and are the only parts subject to rotation in the computational domain. All other boundaries in the domain are defined to be in the lab reference frame, which is stationary.

During start up for this pump, rotation rate changes rapidly from 0 rpm to $\sim$ 1400 rpm. The start-up curve defining rotation rate during start up is shown in Fig. 3. A user-defined field function is used to generate a spline that interpolates between each point in the curve of Fig. 3. This custom field function defines the rotation rate of the rotating reference frame in time.

A mass flow inlet condition is specified for the inlet surface. Both the volume fraction of the phases and mass flow are defined on this type of boundary condition. The inlet is simply defined to be fully liquid, but the mass flow is somewhat more complex. As this impeller changes rotation rate with time, inlet mass flow must also change with time as flow through the pump increases with increasing rotational rate. A table defining mass flow in increments of 0.0002 s is input to the inlet boundary condition and defines the mass flow rate profile. Star-CCM+ automatically generates a spline to interpolate between discrete table values to define inlet mass flow at any point in the considered time range.

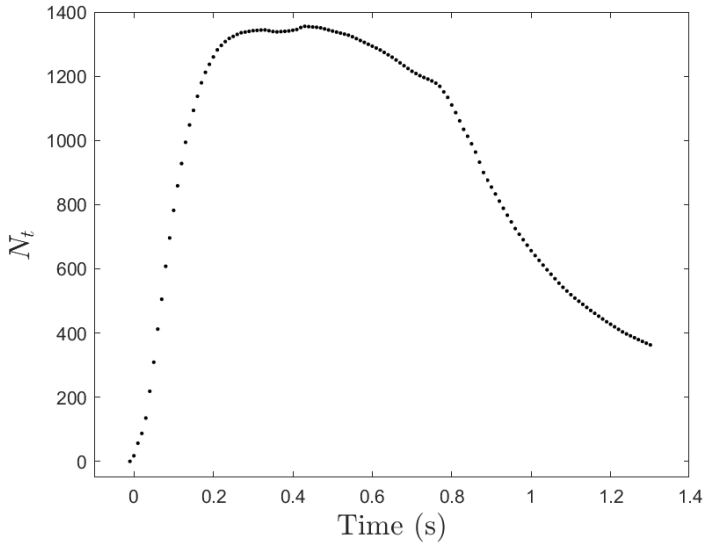

FIGURE 3: Impeller rotation rate during start-up for the considered pump.

The radial outlet surface is defined as a pressure outlet. This type of boundary condition requires a static pressure definition as well as a volume fraction definition. As with the inlet boundary, the volume fraction at the outlet is defined to be fully liquid. While pressure outlets define pressure on the outlet boundary, they are also used to control inlet boundary pressure. The outlet pressure less the head rise produced by the impeller then becomes the inlet pressure. As the considered impeller is meant to operate at a constant inlet total pressure during start-up, the defined static pressure at the outlet boundary must vary with time as pump head, which dictates the difference between inlet and outlet boundary pressures, is dependent on the transient rotational rate.

To determine how outlet static pressure must change

with time to maintain a constant inlet total pressure, a non-cavitating simulation with constant outlet pressure is run to generate pressure and velocity field estimates for the full computational domain. The non-cavitating constant outlet pressure simulation data provides inlet total and outlet static pressure curves through the start-up process. The difference between inlet total pressure and target inlet total pressure then acts as a map for how outlet static pressure must change to maintain a constant inlet total pressure.

A table consisting of outlet pressure modified by the difference between actual inlet total pressure and target inlet total pressure in time is used to define the outlet boundary condition of a new simulation that also models cavitation formation. As with the inlet mass flow boundary, Star-CCM+ is able to generate a spline to interpolate between outlet static pressure table values to define outlet pressure at any point in time. After completion of the cavitating simulation with varying outlet pressure, the resulting inlet total pressure data is used to generate another table of revised outlet pressures. Continuing to revise the static pressure data used to define the outlet boundary condition further improves inlet total pressure consistency through time. The process of iterating through simulations to refine the outlet static pressure based on the inlet total pressure data of the previous simulation is outlined in Fig. 4. This iterative process is completed four times in total for this work, with inlet total pressure continuing to approach the constant target value with each iteration. For ease of identification, each simulation performed for this work is named. Iteration 0 corresponds to the non-cavitating simulation with constant outlet pressure. Iterations $1-4$ are all cavitating simulations with varying outlet static pressure. For Iterations $1-4$, outlet static pressure refinement improves with increasing iteration number.

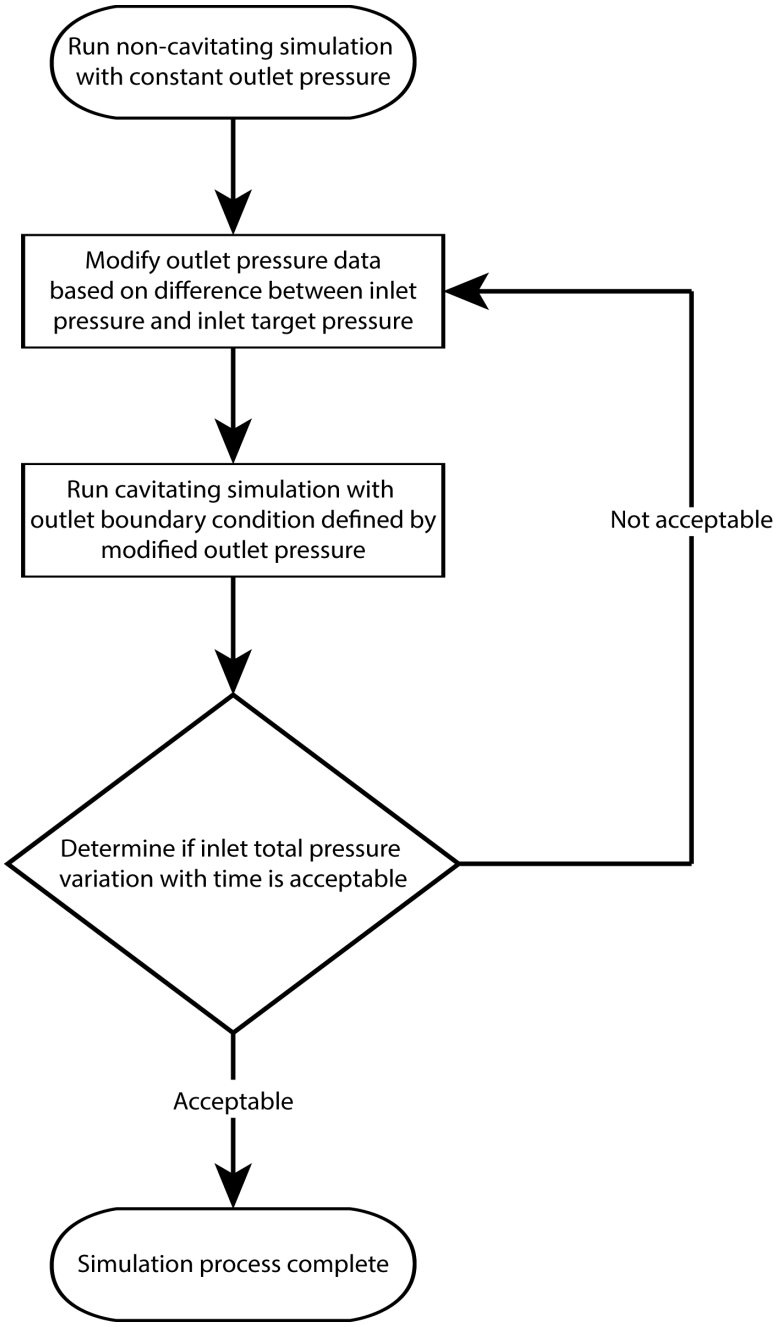

FIGURE 4: Flow chart describing simulation iteration process.

2.5 Processing

To capture the transient flow physics generated by transient start up, all simulations must employ an unsteady solver. Therefore, a time step, inner iterations and the maximum physical time must be defined.

For Iterations 1-3 presented here, a time step of 1×10^{-4} was used with 20 inner iterations per time step. However, a numerical error caused Iteration 2 to prematurely stop at 0.63 s of the full 1.3 s start-up time. The time step was then reduced to 1×10^{-5} for Iterations 3 and 4. The reduced time step prevented any further numerical errors. The time step of 1×10^{-4} corresponds to 0.8° of rotation per time step at the highest rotational speed, while the revised time step of 1×10^{-5} corresponds to 0.08° of rotation per time step at the highest rotational speed. Prior work

centered around similar situations has shown that a time step resulting in 0.5° of rotation per time step is sufficiently small for good simulation convergence [20], however, this work required a smaller time step to avoid numerical instabilities.

The maximum physical time is defined by the start-up rotation curve. The full start-up can be seen in Fig. 3, and defines maximum physical time for all simulations to be 1.3 s.

3 RESULTS

The main feature of the method of iterating through simulations to approach a constant inlet total pressure presented here is adjusting the pressure outlet boundary condition based on the inlet total pressure data of the previous simulation iteration. Figure 5 shows the normalized difference between inlet total pressure and target inlet total pressure during start-up for each simulation iteration. Iteration 0 is a single phase constant outlet pressure simulation. Iteration 1 is a cavitating simulation that builds on iteration 0 and uses the inlet total pressure data to modify the defined static pressure on the outlet boundary condition. Iteration 2 is also a cavitating simulation and uses the data from Iteration 1 to modify the outlet pressure once again. Iteration 3 is a cavitating simulation, and follows the same process and uses data from Iteration 2 to modify outlet static pressure. Iteration 4 is a cavitating simulation and uses the data from Iteration 3 to modify outlet static pressure again.

As seen in Fig.5, and as should be expected, the inlet total pressure difference varies wildly from the target inlet total pressure in Iteration 0. Inlet total pressure is initially much higher than the target, but drops rapidly, and falls below the target from 0 - 0.2 seconds. Inlet total pressure then increases back up to approximately the starting value from 0.2 to 1.3 s. The average error between actual and target inlet total pressure for Iteration 0 during start-up is 118%. As head coefficient and rotational rate are directly related, and as outlet pressure for Iteration 0 is constant through start-up as seen in Fig. 6, inlet total pressure changes drastically to accommodate the transient rotational rate.

The inlet total pressure trend of Iteration 1 is significantly different than that of Iteration 0 due to the changing outlet pressure based on the inlet total pressure of Iteration 0. The inlet total pressure difference between actual and target of Iteration 1 is essentially constant and negligible

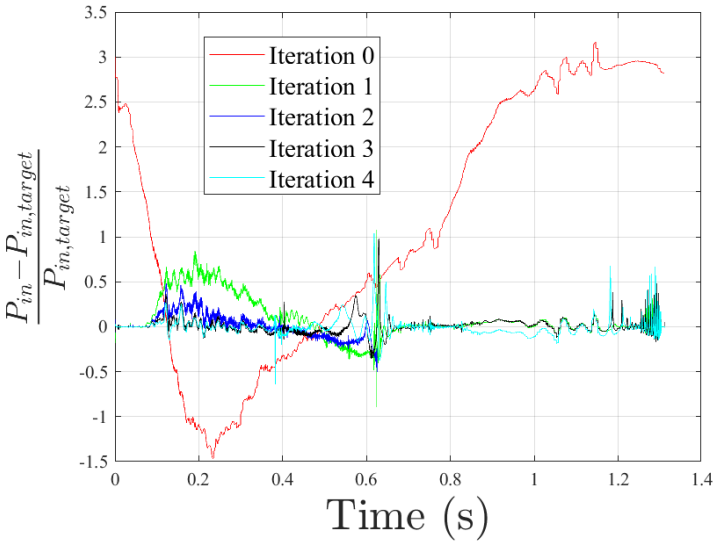

FIGURE 5: Normalized difference between actual inlet total pressure and target inlet total pressure during start-up for each simulation iteration

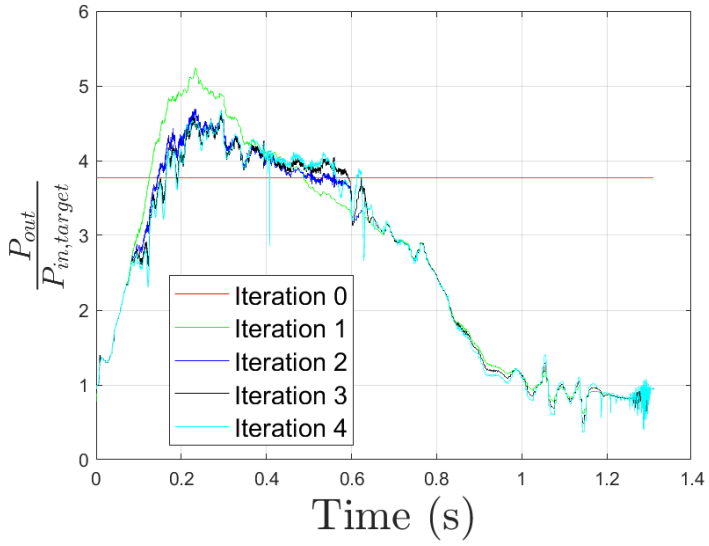

FIGURE 6: Normalized outlet static pressure during start-up for each simulation iteration

between 0 and 0.08 s. Pressure difference increases the error between actual and target inlet total pressure to 49% on average between 0.08 and 0.25 s after which it returns back to approximately 0 at 0.7 s, where it remains until it oscil-

lates rapidly from 1.2 to 1.3 s. The average error between actual and target inlet total pressure for Iteration 1 during the full start-up is 2.59%. As can be seen in Fig. 6, the defined pressure on the outlet boundary condition varies with time to counteract the inlet total pressure changes in Iteration 0. For Iteration 1, outlet pressure increases sharply from 0 to 0.23 s, and decreases from 0.23 to 1.3 s.

Inlet total pressure difference more closely approximates a constant value with no difference between target and actual pressure during the full start-up with Iteration 2. The deviation from target pressure from 0.2 to 0.7 s seen in Iteration 1 decreases by up to 75% in Iteration 2 which results in an average error of 1.29% from 0 to 0.63 s. However, as can be seen in Fig. 5, the inlet total pressure data for Iteration 2 ends at 0.63 s. This simulation iteration experienced a numerical error at this point, preventing simulation completion. The incomplete outlet pressure data of Iteration 2 is seen in Fig. 6. Outlet pressure corresponding to Iteration 2 exhibits an average decrease of 3.6% when compared to Iteration 1 from 0 to 0.63 s. Despite the incomplete status of this simulation, the inlet pressure data from 0 to 0.63 s provides useful information that is used to modify the outlet pressure definition for Iteration 3.

To prevent additional numerical errors, the time step for Iteration 3 was decreased by an order of magnitude. While simulation run time increased, the simulation ran to completion. As seen in Fig. 5, the inlet pressure difference for Iteration 3 is slightly better than Iteration 2, with an average reduction in inlet total pressure of 2.4% between 0 and 0.4 s. However, from 0.5 to 0.6 s, there is a $\sim 4\%$ average increase in inlet pressure difference of Iteration 3 over Iteration 2. After 0.6 s, the inlet pressure difference for Iteration 3 closely follows that of Iteration 1, with the same oscillation from 1.2 to 1.3 s. The average error between inlet total pressure and target inlet total pressure for Iteration 3 during the full start-up is 1.56%. As seen in Fig. 6, the outlet pressure of Iteration 3 closely follows, but is slightly lower than that of Iteration 2, corresponding to a 3.6% decrease, on average, from 0 to 0.63 s. From 0.63 to 1.3 s, the outlet pressure of Iteration 3 closely follows that of Iteration 1, with an average decrease of 4.8%.

Using the data from Iteration 3 to generate a new commanded outlet pressure trace, shown in Fig. 6, results in the curve corresponding to Iteration 4, which has an average decrease of 21% when compared to that of Iteration 3. The improved outlet pressure definition causes an average inlet pressure difference error of 1.27% for Iteration 4 during startup. Using the method of controlling simulation inlet total pressure during start-up described in the methods section above, average error during start-up dropped from 118% to 1.27% in five simulation iterations.

Figure 7 plots pump head coefficient through the start-up process. Each simulation iteration predicts approximately the same result, with only a 7% decrease on average between Iteration 0 and Iteration 4 from 0 to 1 s. From 1 to 1.3 s, head coefficient exhibits strong oscillations due to pressure fluctuations caused by cavity formation and collapse. Head coefficient is a non-dimensional measure of the pump performance, and describes the difference between inlet and outlet boundaries, which is why it varies so little between Iteration 0 and Iteration 4.

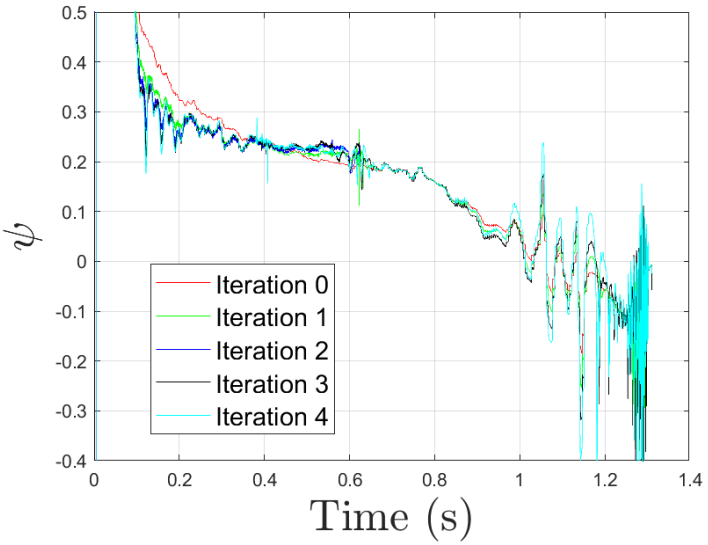

FIGURE 7: Head coefficient produced by the impeller during start-up for each simulation iteration

Cavity formation is shown in Figure 8, which plots total cavity volume in the computational domain during start-up. In all simulation iterations, cavity volume rapidly increases from 0.08 to 0.22 s, after which it decreases to approximately zero cavity volume at 0.65 s. Rapid cavity volume increases correspond directly to the region of greatest rotational acceleration in the start-up curve. The vapor collapse at 0.65 s causes inlet pressure fluctuations that are evident in Fig. 5, and increase the difficulty of maintaining a

constant inlet total pressure. The formation of another cavity occurs at 0.86 s and dissipates at 1.244 s. This cavity is different from that occurring from 0.08 to 0.22 s, in that it forms on the pressure side of the blade and at the blade tips rather than on the typical suction side. Both cavity volume nodes exist in all cavitating simulations, but cavity volume increases with increasing simulation iteration. Iteration 3 and 4 agree within 5% of the cavity volume between 0.08 and 0.22 s. However, Iteration 4 predicts cavity volume between 0.86 and 1.22 s to be up to 79% greater but on average 13% greater than Iteration 3.

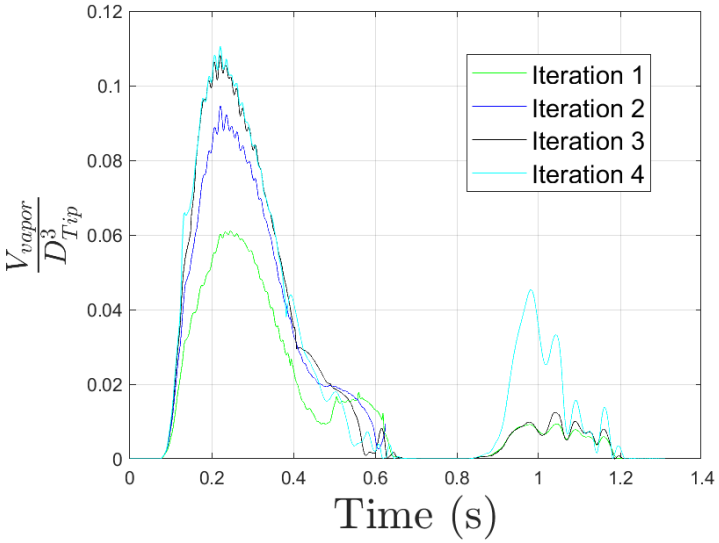

FIGURE 8: Normalized cavity volume during start-up for each simulation iteration

The second node of cavitation formation from 0.8 to 1.2 s is a function of fluctuating flow coefficient affecting incidence and causing flow separation. Figure 9 plots flow coefficient through the pump during start-up. Flow coefficient varies between Iteration 0 and 1, but seems to converge on a solution for Iterations 2, 3, and 4, with an average decrease of 1.8% from Iteration 3 to 4. For these simulations, flow coefficient increases rapidly from 0 to 0.4 s, which is when the impeller reaches the maximum rotational velocity. From 0.4 to 0.8, flow coefficient continues to increase, but at a lesser rate as the impeller is decelerating. From 0.8 to 1.3 s, flow coefficient begins to increase again, at a 95% greater slope than that from 0.4 to 0.8 s. The increasing flow through the pump must cause the flow angle at the leading edge to increase so much such that it causes flow separation on the pressure side of the impeller blades.

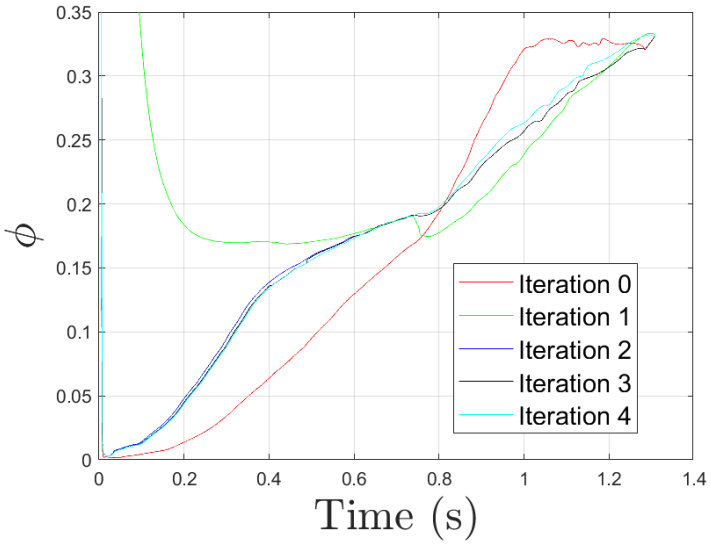

FIGURE 9: Resulting flow coefficient for the impeller during start-up for each simulation iteration

Figure 10 plots the normalized RMS force on the impeller during start-up. Force magnitudes vary widely from Iteration 0 to Iteration 4, but Iterations 2, 3, and 4 seem to agree well, suggesting that a reasonably converged force solution is reached. However, average difference between the RMS forces of Iterations 3 and 4 is 87%. This is a function of the increased cavitation in Iteration 4 causing force fluctuations, which increases the average difference. In Iteration 4, RMS force initially drops from 0 to 0.13 s. An increase in force occurs from 0.13 to 0.28, which corresponds to the rapid formation of cavitation. Forces then decrease to approximately 0 at 0.48 s and remain there until 0.64 s. Large force fluctuations, similar to those seen in the inlet and outlet pressure plots (Figs. 5 and 6), are evident at 0.64 s due to cavitation collapse. Forces then increase to a maximum until 0.95 s, which is maintained at an approximately constant level until 1.3 s. The fluctuations from 1 to 1.3 s are caused by cavitation volumes forming on the pressure side of the blades, which loads and unloads the impeller.

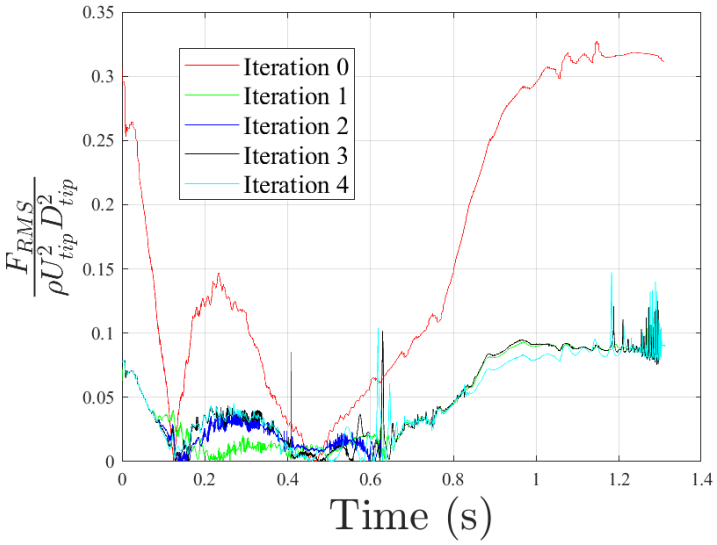

FIGURE 10: Normalized RMS force on the impeller during start-up for each simulation iteration

4 CONCLUSIONS

This work described a method to simulate the transient start-up of a centrifugal impeller using CFD. This method consists of using a non cavitating simulation to generate a typical inlet pressure data trace for a pump. The difference between the inlet total pressure data and the target inlet total pressure is then used to adjust the defined static pressure on the outlet boundary condition in an effort to maintain a constant inlet total pressure in a cavitating simulation. Inlet total pressure is not constant during the first iteration of the cavitating simulation, so a second iteration of the cavitating simulation is completed using the difference between inlet total pressure of the first cavitating simulation and the target inlet total pressure. This difference is again used to adjust the defined outlet static pressure. The process of iterating through simulations modified using inlet total pressure difference data from the previous simulation was completed 4 times for this work. Reasonable agreement between simulation Iterations 3 and 4 for inlet total pressure, head coefficient, cavitation volume, flow coefficient, and RMS forces on the impeller suggest that a reasonable solution was achieved in 5 total simulation iterations.

Cavitation formation and collapse dominates the flow physics of this pump during start-up. During the initial rapid rotational acceleration of the pump, large cavity volumes form, but rapidly collapse as rotational speed stabilizes for a short time. This rapid formation and collapse of vapor induces pressure fluctuations that strongly affects the pressure field and also imparts large rotordynamic forces to the impeller. In addition to the primary cavitation formation when the pump experiences the greatest rotational acceleration, a secondary cavity changes forms on the pressure side of the impeller blades as a result of incidence changes. Corresponding pressure fluctuations and a large increase in rotordynamic forces accompany the formation and collapse of the secondary cavity.

While this simulation method seems to accurately model the complex flow during a transient start up, additional work should be done to further verify the data presented here and validate the method. Additional simulation iterations should be completed and compared to previous simulation iteration data to determine if a converged solution has been reached. More importantly, experimental data of a pump during fast start up must be obtained and compared to simulation data for the same pump. This would provide an absolute measure of the accuracy of the simulation method set forth here.

ACKNOWLEDGMENT

This work was funded in part by the Utah NASA Space Grant Consortium and Concepts NREC.

REFERENCES

[1] Lefebvre, P., and Barker, W., 1995. "Centrifugal pump performance during transient operation". *Journal of Fluids Engineering,* ***117***(1), March, pp. 123–128.

[2] Dazin, A., Caignaert, G., and Bois, G., 2007. "Transient behavior of turbomachineries: Applications to radial flow pump startups". *Journal of Fluids Engineering,* ***129***, pp. 1436–1444.

[3] Tsukamoto, H., and Ohashi, H., 1982. "Transient characteristics of a centrifugal pump during starting period". *Journal of Fluids Engineering,* ***104***, pp. 6–14.

[4] Picavet, A., and Barrand, J., 1996. "Fast start-up of a centrifugal pump - experimental study". In Pump Congress.

[5] Saito, S., 1982. "The transient characteristics of a

pump during start up". *Bulletin of the JSME,* ***25***(201), March, pp. 372–379.

[6] Barrand, J., Ghelici, N., and Caignaert, G., 1993. "Unsteady flow during the fast start-up of a centrifugal pump". In Pumping Machinery, Vol. 154 of *ASME FED*.

[7] NguyenDuc, J., Kaenel, A. V., and Danguy, F., 1993. "Transient behavior of liquid hydrogen pumps during start-up and shutdown of rocket engines". In Pumping Machinery, Vol. 154 of *ASME FED*.

[8] Zhang, Y., Zhu, Z., Jin, Y., Cui, B., Li, Y., and Dou, H., 2013. "Experimental study of a centrifugal pump with an open impeller during startup period". *Journal of Thermal Science,* ***22***(1), pp. 1–6.

[9] Tsukamoto, H., Yoneda, H., and Sagara, K., 1995. "The response of a centrifugal pump to fluctuating rotational speed". *Journal of Fluids Engineering,* ***117***, pp. 479–484.

[10] Tanaka, T., and Tsukamoto, H., 1999. "Transient behavior of a cavitating centrifugal pump at rapid change in operating conditions - part 2: Transient phenomena at pump startup/shutdown". *Journal of Fluids Engineering,* ***121***(4), December, pp. 850–856.

[11] Tanaka, T., and Tsukamoto, H., 1999. "Transient behavior of a cavitating centrifugal pump at rapid change in operating conditions - part 3: Classifications of transient phenomena". *Journal of Fluids Engineering,* ***121***(4), December, pp. 857–865.

[12] Duplaa, S., Coutier-Delgosha, O., Dazin, A., Bois, G., Caignaert, G., and Roussette, O., 2008. "Cavitation inception in fast startup". In The Twelfth International Symposium on Transport Phenomena and Dynamics of Rotating Machinery - ISROMAC-12, pp. 124–133.

[13] Bolpaire, S., Barrand, J., and Caignaert, G., 2002. "Experimental study of the flow in the suction pipe of a centrifugal pump impeller: Steady conditions compared with fast start-up". *International Journal of Rotating Machinery,* ***8***(3), pp. 215–222.

[14] Duplaa, S., Coutier-Delgosha, O., Dazin, A., Bois, G., and Caignaert, G., 2010. "Experimental characterization and modelling of a cavitating centrifugal pump operating in fast start-up conditions". In 13th International Symposium on Transport Phenomena and Dynamics of Rotating Machinery - ISROMAC-13, pp. 22–29.

[15] Duplaa, S., Coutier-Delgosha, O., Dazin, A., Bois, G., and Caignaert, G., 2010. "Experimental study of a cavitating centrifugal pump during fast startups". *Journal of Fluids Engineering,* ***132***(2), February, p. 12.

[16] Matteo, F. D., Rosa, M. D., and Onofri, M., 2011. "Start-up transient simulation of a liquid rocket engine". In 47th AIAA/ASME/SAE/ASEE Joint Propulsion Conference and Exhibit.

[17] Roache, P., 1997. "Quantification of uncertainty in computational fluid dynamics". *Annual Review Fluid Mechanics,* ***29***, pp. 123–160.

[18] Slater, J., 2008 (accessed 7 June, 2017). "Examining spatial (grid) convergence". *NPARC Alliance CFD Verification and Validation Web Site*.

[19] Hirt, C., and Nichols, B., 1981. "Volume of fluid (vof) method for the dynamics of free boundaries". *Journal of Computational Physics,* ***39***, pp. 201–225.

[20] Lundgreen, R., Maynes, D., Gorrell, S., and Oliphant, K., 2019. "Increasing inducer stability and suction performance with a stability control device". *Journal of Fluids Engineering,* ***141***.

[21] CD-Adapco, 2015. "Help files, star-ccm+ version 11.04".